PERGAMON

International Journal of Solids and Structures 39 (2002) 3717–3739

INTERNATIONAL JOURNAL OF SOLIDS and STRUCTURES

www.elsevier.com/locate/ijsolstr

Nonlinear interaction of geometrical and material properties in sandwich beam instabilities

L. Léotoing, S. Drapier *, A. Vautrin

Mechanical and Materials Engineering Department, SMS Division, École, Nationale Supérieure des Mines de Saint-Étienne, 158 Cours Fauriel, 42023 Saint-Étienne Cedex 02, France

Received 13 February 2002

Abstract

The first part of this paper is dedicated to the analytical and numerical characterization of local and global sandwich beam instabilities in a perfect linear framework. Analytical loads are extracted from an original unified model and used to understand in depth, through a parametric study, the role played by each geometrical and material parameter in the development of global as well as local instabilities. Also, the effects of the combinations of these characteristics is used to draw precious design indications. A low CPU time-consuming simplified model is then built and assessed. Critical loads and wavelengths computed from this model are shown to correlate very well with analytical predictions. It is established that this first approach is essential in order to lead to more detailed investigations in a numerical nonlinear framework which is the aim of the second part. The first geometrical nonlinear investigations in which linear elastic materials are considered permit to isolate sandwich configurations developing super- or sub-critical post-buckling behaviours. As a general trend, unstable behaviours are rather related to the occurrence of geometrical localizations along the beam. This is illustrated by the drastic effects of the so-called interactive buckling onto the whole stiffness of the sandwich beam. Moreover, it is shown that sandwiches are very sensitive towards imperfection sizes and forms. Eventually, an elastoplastic constitutive law is introduced for the core. It is demonstrated that plastic flow and strain localization in the core, combined with the occurrence of instabilities, are associated with a drastic drop in the global beam stiffness and with a strong decrease of the maximum limit load for some cases. The phenomenon of shear crimping is also observed which can be assimilated to a post-bifurcated development of the global buckling mode.

Keywords: Sandwich structure; Linear buckling loads; Scale effects; Post-buckling stability; Elastoplasticity; Imperfection sensitivity

1. Introduction

Sandwich structures have been widely used in aeronautics and astronautics since the early 1940s. The first theoretical works dedicated to the mechanical study of these materials are contemporary of their first applications (Williams et al., 1941). In the 1960s, the sandwich behaviour began to be studied in more detail

* Corresponding author. Tel.: +33-04-77-42-00-79; fax: +33-04-77-42-02-49.
E-mail address: drapier@emse.fr (S. Drapier).

0020-7683/02/$ - see front matter
PII: S0020-7683(02)00181-6

such as in the book by Allen (1969), which sets the basis of the mechanics of sandwich structures. But it is actually from the mid 1980s that the use of sandwich structures has moved from classical applications (sandwich are ideally employed as lagging or floor elements) towards structural components, and thus spread in other fields of engineering. The key point in using sandwich structures is the possibility of largely reducing weights while keeping the same equivalent stiffnesses. Then, it is mostly in transportations that their use leads to substantial weight savings straightfully translated into pay loads. This on-going spreading relies first on a better understanding of the mechanisms driving the response of such structures, and second on new manufacturing processes and materials which permit to build some integral parts out of structural units with sandwiches.

Unfortunately, since structural applications undergo multiaxial loadings, the design of sandwich structures must take into account various loadings such as bending, tension, compression, etc. Usually, classical layered material theories are sufficient for describing some of these mechanical sandwich behaviours. However, the heavy material and geometrical heterogeneity of the sandwich structures can be responsible for the existence of scale effects. More particularly the complex response under in-plane compressive loadings still presents some difficulties for designers. Indeed, under such a destabilising loading, the assembly of very different compounds involves the (co-)existence of buckling at two distinct scales: at the global scale of the assembly and at the local scale of the skins and core. For the global scale, the geometrical instability is similar to Euler's buckling for homogeneous beams (Fig. 1a). For the local scale, two forms are generally considered, which are the symmetrical mode (Fig. 1b) and the antisymmetrical mode (Fig. 1c), both corresponding to the local buckling of skins commonly referred to as wrinkling.

Then the complete understanding and characterization of buckling in such materials require to take into consideration geometrical instabilities at the two scales of observation. Since the mid of the last century, numerous theoretical studies have been conducted on buckling in sandwich beams, panels and shells (Williams et al., 1941; Allen, 1969; Vinson, 1989). The classical approach developed so far is to propose two distinct models associated, respectively, with the study of global and local buckling in an uncoupled way. The global mode of a sandwich beam is studied, thanks to an equivalent homogeneous beam in which the transverse shear effects must be considered. For the local forms, a beam (skin) resting on an elastic foundation (core), able to model the transverse normal and shear stiffnesses of the core, is generally used. The classical formula for the two local forms is given by Eq. (1), where E_c, G_c and E_s are material parameters standing, respectively, for the core transverse normal modulus, the core transverse shear modulus and the skin Young's modulus

$$\sigma_{\text{class}} = Q\sqrt[3]{E_c G_c E_s}. \tag{1}$$

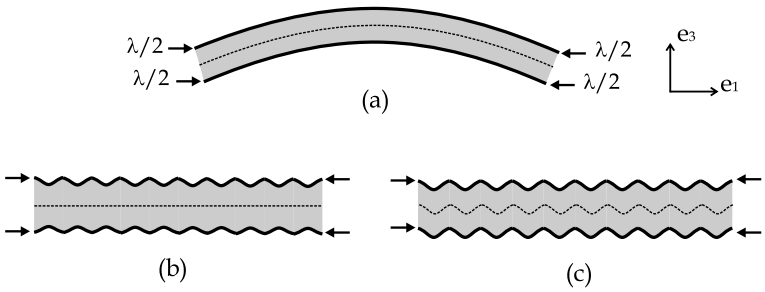

Fig. 1. Sandwich buckling at two scales: (a) global buckling (Euler's type), (b) symmetrical wrinkling of the skins, (c) antisymmetrical wrinkling of the skins.

The value of constant Q varies from 0.4 to 0.9 depending on the authors and the wrinkling case studied (Allen, 1969). The very simplified form of Eq. (1) and the considerable uncertainty concerning the value of Q both demonstrate the difficulty in characterizing instabilities in such structures. These approaches are often intuitive and only appropriate for special cases. Trying to clarify these approaches with experimental results would be of little use since experiments on buckling are by nature unstable and usually only the resulting failure can be observed. In the literature, very few studies are dedicated to the experimental characterization of wrinkling, and correlation can hardly be attempted with the theoretical approaches, unless assigning a variable character to the constant Q as suggested by Teti and Caprino (1989).

Then there is a need for more comprehensive modelling approaches able to first describe the different mechanisms prevailing at each scale, and second to account for a potential interaction of these instabilities at the two scales. Indeed, an optimization of sandwich structures against buckling at the two scales will lead to configurations where these buckling modes will appear at almost the same critical load (Byskov and Hutchinson, 1977). Such configurations will present an unstable post-buckling behaviour resulting of the combination of a global and a local mode (Hunt et al., 1988; Byskov and Hutchinson, 1977). Also these optimum configurations will tend to be very imperfection-sensitive. Some recent studies deal with the notion of interactive buckling but they remain very seldom and all present important limitations. They can be classified into two distinct classes, the analytical and semi-analytical approaches (Hunt et al., 1988; Sokolinsky and Frostig, 1999) and the numerical ones (Starlinger, 1990).

Eventually, it clearly appears that there is a real need for simple but reliable and rich design tools enabling to make rapid calculations for the use of sandwich materials in structural units. Our first aim is to develop a unified sandwich beam model able to grasp both local and global instabilities in a perfect framework. These analytical results are essential for the mechanical understanding of local and global phenomena, by getting an insight into the role played by the combinations of geometrical and material parameters at both scales. Through the analytical expressions associated with the three main forms of instability (Fig. 1), simple design diagrams can be established and sandwich configurations can be quickly selected against local and global buckling. Even if rich conclusions can be drawn in this very simple but mechanically rigorous framework, it is not sufficient for a complete description of the sandwich buckling behaviour. The second step is therefore to build a coherent finite element model in order to conduct rapid numerical investigations including geometrical and material nonlinearities, in other words in a more realistic framework. Finally, this well-founded numerical tool can be reliably used and nonlinear geometrical analyses with linear elastic materials are first led. They permit to identify the different post-buckling paths and isolate the buckling modes susceptible to develop super- or sub-critical regimes. The notion of interactive buckling is also described and it is shown, in agreement with Byskov and Hutchinson (1977), that the interaction between a global curvature and local wrinkling of the compressive skin induces a drop in the global stiffness of the beam. In the last part, more realistic calculations with a crushable core material (foam) show that the imperfection sensitivity of sandwich structures is still emphasized when plastic strains can develop, which lead to very sub-critical responses.

2. Linear buckling loads: analytical and numerical investigations

In this section, an analytical model is presented whose unified formulation and well-founded mechanical assumptions permit to establish reliable design criteria for the three main forms of instability. The accuracy of the corresponding predictions is assessed by FE evaluations. It is shown that these analytical expressions represent precious guides for the configuration selection of sandwich and for the use of an accurate numerical tool with low CPU time-consumption.

2.1. Analytical eigenvalues and design rules

2.1.1. Unified model

The following unified model is described in more detail in Léotoing et al. (2001a). For the sake of simplicity, a symmetrical sandwich beam of length L and width b is considered. Both skins and core are made up of homogeneous isotropic linear elastic materials, defined, respectively, by their Young's modulus E_s and E_c, and its shear modulus G_c for the core. Other notations used subsequently correspond to those introduced in Fig. 2. The model is formulated in displacements, consequently the main difficulty lies in the choice of proper kinematics, which must be rich enough to observe both global and local instabilities but simple enough to yield tractable closed form solutions. A higher-order theory is required in the core since it was shown to represent well the mechanical behaviour of short wavelength phenomena (Lo et al., 1977). For the skins, a simple Euler–Bernoulli beam model is used. By considering perfect skin/core interfaces and a linear transverse shear stress distribution across the beam thickness, the core displacement field $(\mathbf{u}^c(\mathbf{x}) = u_1^c(\mathbf{x})\mathbf{e}_1 + u_3^c(\mathbf{x})\mathbf{e}_3)$ can be written, thanks to the unknown displacements of the top $(\mathbf{u}^t(x_1))$ and bottom $(\mathbf{u}^b(x_1))$ of the sandwich beam and to a gradient of rotation $(\phi(x_1))$ in the core (Eq. (2))

$$\begin{aligned} u_1^c(x_1,x_3) &= \frac{(x_3-t_s)}{t_c}u_1^t(x_1) + \left(1-\frac{(x_3-t_s)}{t_c}\right)u_1^b(x_1) + t_s\left(\frac{x_3-t_s}{t_c}\right)u_{3,1}^t(x_1) \\ &\quad - t_s\left(1-\frac{(x_3-t_s)}{t_c}\right)u_{3,1}^b(x_1) + \frac{1}{6}(2x_3-t)(x_3+t_s-t)(x_3-t_s)\phi_{,1}(x_1), \\ u_3^c(x_1,x_3) &= \frac{(x_3-t_s)}{t_c}u_3^t(x_1) + \left(1-\frac{(x_3-t_s)}{t_c}\right)u_3^b(x_1) + (x_3-t_s)(-x_3+t_s+t_c)\phi(x_1). \end{aligned} \tag{2}$$

Then, using this displacement field, the corresponding stresses can be associated with through the linear constitutive laws. Stresses are represented by the second Piola–Kirchhoff tensor and strains by the Green–Lagrange tensor limited to the moderate rotation terms. Eventually, for a simply supported sandwich beam, a non-linear system of five differential governing equations is derived from the Principle of Virtual Works. Since the buckling loads of both the linearized and nonlinear problem coincide (Leger et al., 1998), a linearized form of the previous system is sufficient to determine those loads. The linearization is achieved by postulating a linear pre-buckling state which still holds at the occurrence of the first geometrical instability. Consequently, membrane and moment resultants depend on membrane strains only, and the whole governing equations become linear. The critical loads of this problem are the eigenvalues of the corresponding eigenproblem.

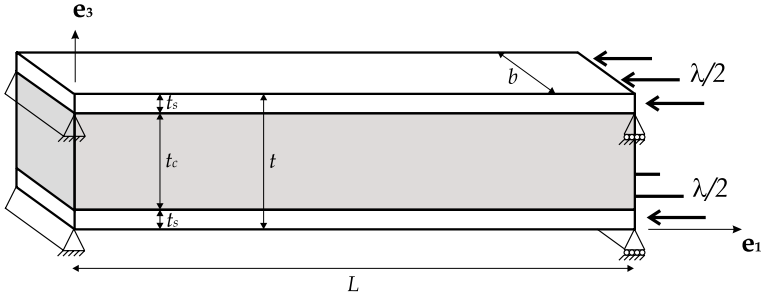

Fig. 2. Notations for a simply supported sandwich beam.

2.1.2. Analytical expressions

The formal resolution of the eigenproblem leads to two strictly positive eigenvalues corresponding, respectively, to an antisymmetrical eigenmode and to a symmetrical one. Through this calculation, three buckling modes and the corresponding loads (λ_X^{um}) can be isolated. Indeed, the eigenvalue associated with the antisymmetrical mode can correspond to the occurrence of either global (critical wavenumber is 1) (Eq. (3)) or local (high critical wavenumber—wrinkling) buckling (Eq. (4)), depending on the sandwich configuration. Moreover, for some combinations of geometrical and material parameters, the antisymmetrical wrinkling does not exist. A relationship (Eq. (4)) between the different parameters can be determined, the validity of which corresponds to the possible existence of this local form of instability. For the symmetrical case, there is only one possible critical load which corresponds to a local mode (Eq. (5)):

$$\lambda_{AG}^{um} = B\left[\frac{\rho_t}{\rho_L^2} + \left(\frac{6_{\rho_E}}{(\rho_t/\rho_v) + (\rho_t/12\rho_L^2) + 2\rho_E\rho_L^2}\right)\left(\frac{1}{\rho_t} + \rho_t + 2\right)\right], \tag{3}$$

$$\lambda_{AL}^{um} = B\left[12\left(\sqrt{2\rho_E\left(\frac{1}{\rho_t} + 2\right)} - \frac{\rho_t}{\rho_v}\right)\right] \quad \text{if} \quad \frac{2\rho_t^3}{\rho_v^2\rho_E(1+2\rho_t)} < 1, \tag{4}$$

$$\lambda_{SL}^{um} = B\left[4\sqrt{6}\sqrt{\frac{\rho_E}{\rho_t}} + \frac{2\rho_E\rho_v}{\rho_t^2}\right], \tag{5}$$

where the dimensionless ratios introduced are some independent combinations of the geometrical and material parameters ($\rho_L = L/(\pi t_c)$, $\rho_E = E_c/E_s$, $\rho_t = t_s/t_c$ and $\rho_v = G_c/E_c$). Factor B common to the three previous equations is expressed as $B = b\rho_t E_s t_s/6$ and has consequently a positive value.

The plots of the stability curves ($E_s = 50,000$ MPa, $E_c = 70$ MPa, $G_c = 25$ MPa, $t_s = 1$ mm, $L = 600$ mm, $b = 40$ mm) for two different core thicknesses (t_c) clearly illustrates the shift between a global and a local antisymmetrical mode (Fig. 3). One must point out that for kinematics with some linear displacement fields in the core, the minimum is always reached for $n = 1$ (Fig. 3), i.e. no antisymmetrical wrinkling can be represented. Fig. 4 represents the change in the critical load of the sandwich beam ($\min(\lambda_{AG}^{um}, \lambda_{AL}^{um}, \lambda_{SL}^{um})$)

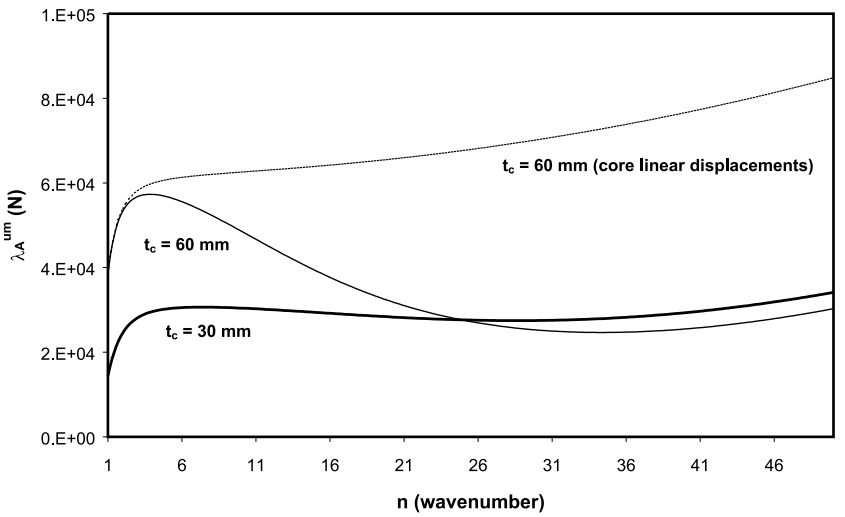

Fig. 3. Neutral stability curves for the critical antisymmetrical load (λ_A^{um}) for two different thicknesses t_c of the core ($t_c = 30$ mm, $t_c = 60$ mm), and for the analytical model based on a linear core displacement.

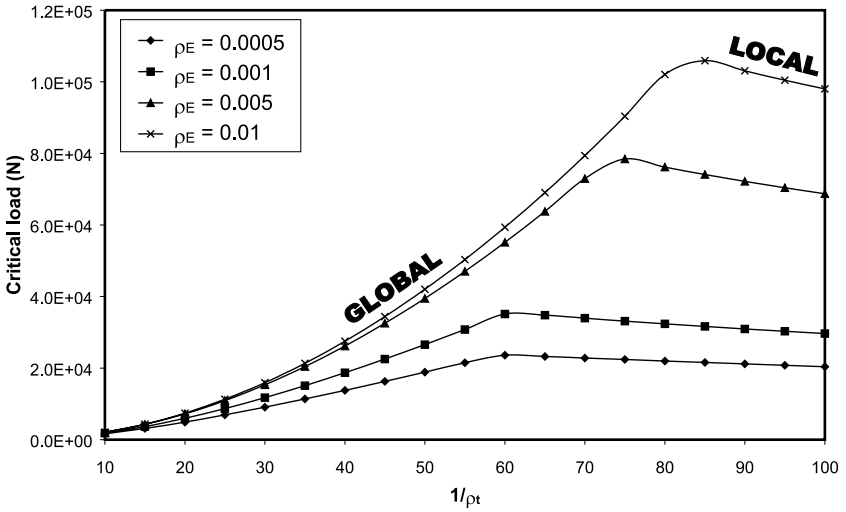

Fig. 4. Change in the critical load of the sandwich beam ($\min(\lambda^{um}_{AG}, \lambda^{um}_{AL}, \lambda^{um}_{SL})$) versus the thickness ratios $1/\rho_t$ and for different modulus ratios ρ_E.

versus the thickness ratios $1/\rho_t$ and for different modulus ratios ρ_E ($E_s = 70,000$ MPa, $t_s = 1$ mm, $L = 1000$ mm, $b = 50$ mm). One can notice that there exist very different configurations for which global or local instabilities will develop at the lowest loads. It clearly appears that the predominance zone of global or local buckling is strongly dependent on the sandwich configuration. Besides, for a fixed modulus ratio, the transition point between the two forms of instability corresponds to an optimized sandwich configuration against buckling. This observation fits a well-known result that the optimum design leads to configurations for which at least two buckling modes will appear at almost the same critical load (Byskov and Hutchinson, 1977). Following these authors, such configurations will present an unstable post-buckling behaviour resulting of the combination of a global and a local mode, and will tend to be very imperfection-sensitive. These configurations will receive a particular attention in the second part of the present contribution.

An alternative consequence of the existence of these instabilities at two scales is the need for designers to identify more systematically the configurations globally or locally unstable. This is achieved by understanding first the role played by each geometrical and material parameter, and second the weight of their combinations. Using the previous analytical expressions of the critical loads offers such a versatility.

2.1.3. Design rules

A sensitivity study was led in Léotoing et al. (2001b). The classical result of the high sensitivity of slender homogeneous beams towards global buckling was clearly demonstrated for sandwich beams. The calculation of the sensitivities for the two local forms are very comparable and their local nature is clearly confirmed by their independence towards the beam length. For the two forms, the key parameter is the thickness of the skins due to its cubic contribution in their flexural stiffness. Thus, t_s is rather associated with the local behaviour of the sandwich beam whereas t_c can be classified as a global parameter. The sensitivities towards the core moduli (E_c, G_c) are rather comparable for the two local modes and confirm the role played by both the transverse normal and shear stiffnesses on the occurrence of local phenomena.

Moreover, graphic tools were proposed (Léotoing et al., 2001b) to localize without any ambiguity the different zones of prevalence, i.e. when global buckling may appear rather than local buckling, and conversely. The three critical loads λ^{um}_{AG}, λ^{um}_{SL} and λ^{um}_{AL} can be compared by pairs, thus defining some zones of predominance for each and every phenomenon by evaluating the sign of the differences. For a given

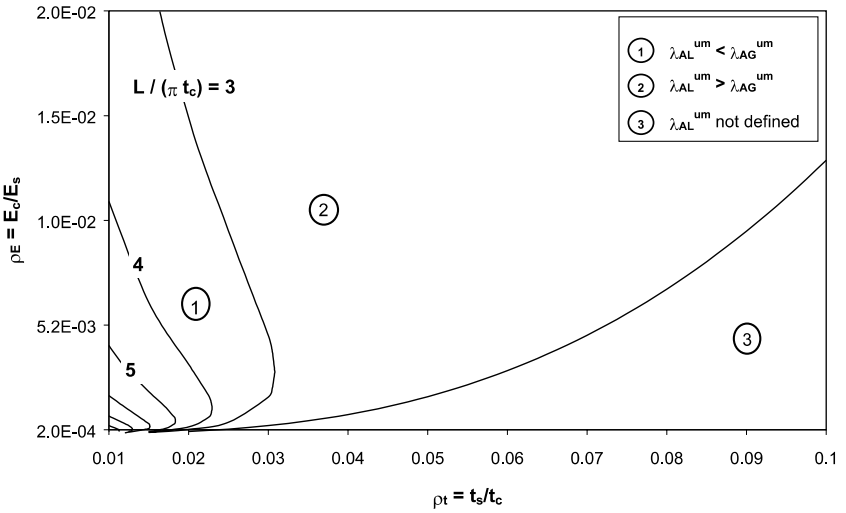

Fig. 5. Change in the predominance zones between antisymmetrical wrinkling and global buckling with $\rho_L = L/\pi t_c$ varying from 3 to 8.

Poisson's ratio, the parameter ρ_v is constant and then the zones can be easily plotted on a ρ_t–ρ_E graph, for different values of ρ_L. For the two local forms, the analysis of the inequality shows that the antisymmetrical wrinkling will unconditionally occur at lower loads than the symmetrical wrinkling, for ordinary engineering materials used in sandwich construction ($2 \times 10^{-4} < \rho_E < 2 \times 10^{-2}$ and $10^{-2} < \rho_t < 10^{-1}$). Then, predominance zones can be plotted for λ_{AG}^{um} and λ_{AL}^{um}, the two loads of interest. The corresponding graphic is given in Fig. 5, for the configuration previously used for Fig. 4. In Fig. 5 one can observe the change in the frontier between the two zones as a function of the slenderness (ρ_l). An additional zone (zone ③ in Fig. 5) is reported that bounds the configurations for which the condition of existence of the antisymmetrical wrinkling (Eq. (4)) is not valid.

Fig. 5 shows that the local forms are predominant in sandwich beam made up of weak and thick core (zone ①—low values of ρ_E and ρ_t). Moreover, one can observe that local instabilities disappear for slender sandwich beams. For a ratio $\rho_L > 10$, without any material consideration, it can be asserted that the sandwich beam will behave in compression as its equivalent homogeneous representation. These diagrams can be useful for a first dimensioning of sandwich beams under in-plane compression and can give some precious information on their buckling behaviour when a material or geometrical configuration is prescribed regarding other loading conditions.

2.2. Numerical eigenvalue buckling predictions

2.2.1. Finite Element sandwich beam model

In the literature, very few F.E. models are dedicated to sandwich modelling, and very rarely justified rigorously. This lack of reference model constrains us to try and use F.E. displacement-based models which intrinsically cannot ensure any stress continuity at the interfaces. Therefore, it is necessary to assess the quality and accuracy of such models. The first point in setting these models is to eliminate the local effects at the edges which induce complex and unrealistic linear buckling modes. Using a multi-point constraint, either edge is constrained to behave as a solid medium, i.e. the nodes are prescribed to move along a straight line connecting the two extreme nodes located on the top and bottom skins (Fig. 6). The line can stretch linearly and rotate around a central node, the degrees of freedom (d.o.f.) of which are used to apply the

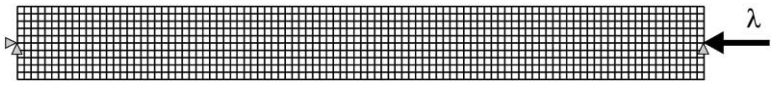

Fig. 6. Simplified F.E. model of the sandwich beam (1200 elements and approximately 2000 d.o.f.).

boundary conditions and loadings. This edge modelling is also suggested by the observation of real configurations of sandwich in which the edges are stiffened by close-outs in order to apply connections or loadings (HEXCEL, 1989).

The first way of modelling the sandwich beam can consist in a two-dimensional model for the whole beam. The skins and the core can be meshed with 4-noded bilinear plane stress solid elements. Various cases tested did not show any significant discrepancy for the eigenbuckling loads calculated with plane strain or plane stress elements. The point in this mesh is rather that in order to have some aspect ratios of the order of the unity, the small elements of the skins induce a large number of elements in the beam length. Then, this model is very heavy and will be CPU time-consuming for future nonlinear analyses. This model can be simplified by replacing the two-dimensional elements of the skins with linear and shear deformable beam elements, which reduces significantly the number of d.o.f. (Fig. 6). The slight loss in the global equivalent flexural stiffness due to the position of the skins that is closer than in the actual sandwich beam is corrected by modifying the beam width.

In this simplified model, the size of the beam elements is no longer controlled by the thickness of the skins, but the number of beam elements must be sufficient to observe the local instabilities. A convergence study has been carried out which showed that the local critical loads are strongly dependent on the length of the beam elements used. For example, Fig. 7 represents the eigenbuckling loads for the sandwich configuration from Table 1 versus the number of beam elements. The local critical loads can be overestimated if too few elements represent the skins, and the global mode becomes 'artificially' critical. Then, in practice, the beam number is selected by prescribing at least 8–10 elements over one wavelength, the expression of which is known analytically.

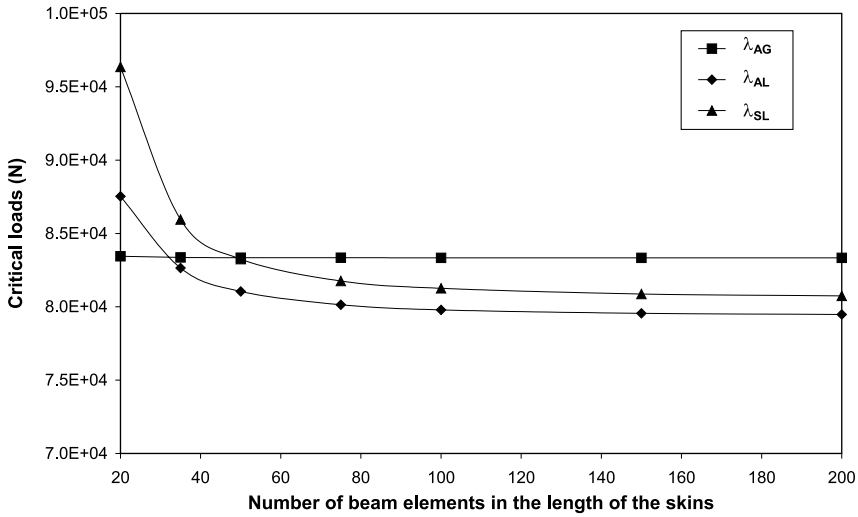

Fig. 7. Change in the three critical eigenbuckling loads versus the number of beam elements along the skins for the simplified model ($t_s = 1.25$ mm).

Table 1
Sandwich characteristics for the comparison between analytical and numerical eigenvalue buckling predictions

E_s (MPa)	70,000	t_c (mm)	50
E_c (MPa)	100	L (mm)	470
G_c (MPa)	35.7	b (mm)	60

A comparison can be made between the two F.E. models. In Table 2 the critical loads associated with the three buckling modes are reported for the simplified model and for two different mesh sizes of the complete model. Also, the total CPU time needed to extract 25 eigenvalues on 450 MHz/2 Gb RAM USparc II Sun workstations is reported. In this comparison, the parameters n_L and n_t stand, respectively, for the number of elements in the length and in the thickness of skins, the sandwich configuration considered is given in Table 1 with $t_s = 1.5$ mm. In Table 2, the global critical load does not vary significantly for the three F.E. models presented, whereas for the local forms the results of the complete model converge towards the critical loads of the simplified model for a large number of elements in the skins. The gain in CPU time for the simplified model is then clearly demonstrated (factor of $\sim$60). Moreover, an evaluation of the energetic contributions of every stress component for the two previous F.E. models have shown very similar behaviours. Consequently it can be assumed that the mechanical behaviour of the sandwich beam is well represented by this low CPU time-consuming simplified model (Léotoing et al., 2001b).

2.2.2. Comparison between analytical and numerical results

The three analytical buckling modes can be found using the previous F.E. model, thanks to an eigenvalue buckling analysis (Fig. 8). Numerical and theoretical critical loads for the antisymmetrical (global and local) and symmetrical (local) mode are plotted versus the thickness ratio, respectively, in Figs. 9 and 10, for the sandwich configuration given in Table 1. In Fig. 9, it can first be noticed the good correlation between analytical and F.E. predictions for the global load and for the antisymmetrical wrinkling mode. The

Table 2
Comparison between the eigenvalue buckling predictions for the two F.E. models

	Simplified model ($n_L = 100$)	Complete model ($n_L = 400$ and $n_t = 3$)	Complete model ($n_L = 1500$ and $n_t = 8$)
d.o.f.	2000	22,000	110,000
CPU time (s)	64	560	3700
λ_{AG} (kN)	83.3	83.8	83.5
λ_{AL} (kN)	79.8	85.6	78.7
λ_{SL} (kN)	81.3	87.7	79.8

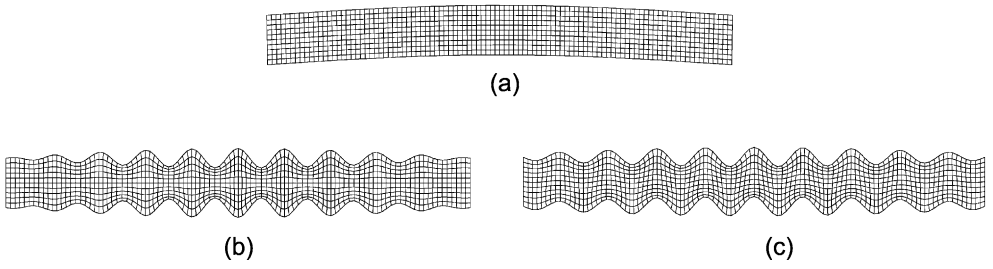

Fig. 8. F.E. beam sandwich buckling modes: (a) global buckling, (b) symmetrical wrinkling of the skins, (c) antisymmetrical wrinkling of the skins.

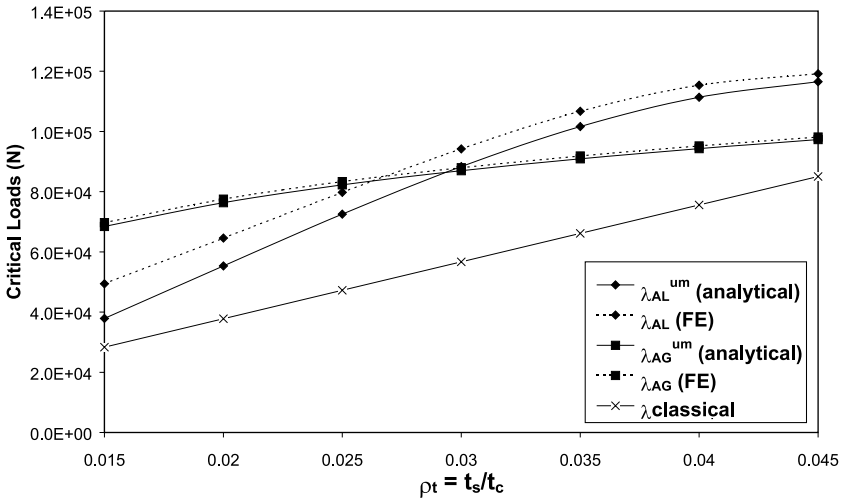

Fig. 9. Change in the analytical and numerical antisymmetrical critical loads for the global and local modes versus the thickness ratio.

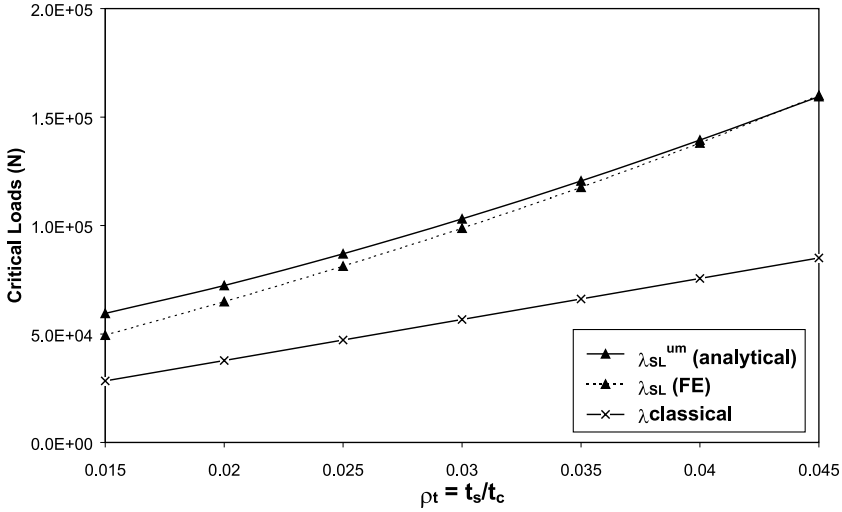

Fig. 10. Change in the analytical and numerical symmetrical critical loads versus the thickness ratio.

discrepancy between the two models does not exceed 22% for the configuration tested. For the symmetrical form (Fig. 10), the agreement is very good (discrepancy lower than 15%) and perfect for high thickness ratios. Anyway, the predictions for both local instabilities correlate rather well when observing the plot of the classical load for a classical and usual value of $Q = 0.5$ (Eq. (1)), the predictions of which are very conservative. The discrepancy between analytical and numerical results can be partly explained by the simplistic analytical shear stress distribution postulated which does not estimate accurately the actual energetic contribution of the shear stress (Léotoing et al., 2001b).

It is also essential to compare the analytical and numerical critical wavelengths. Indeed, if a good correlation is found, a time-optimum mesh will be used by controlling the number of beam elements along the

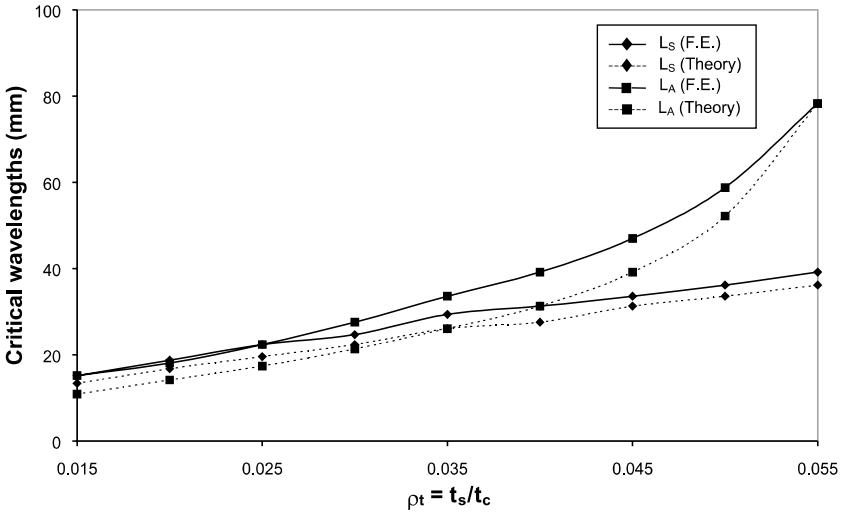

Fig. 11. Comparison between analytical and numerical critical wavelengths.

skins, based on the knowledge of the analytical wavelengths for symmetrical ($L_S = L/n_S$) and antisymmetrical ($L_A = L/n_A$) wrinkling (Eqs. (6) and (7))

$$n_S = \rho_L \sqrt[4]{\frac{24\rho_E}{\rho_t}}, \tag{6}$$

$$n_A = \rho_L \sqrt{6\left(\frac{1}{\rho_t}\sqrt{2\rho_E\left(\frac{1}{\rho_t}+2\right)}-\frac{2}{\rho_v}\right)}. \tag{7}$$

Fig. 11 illustrates the comparison between the two analytical wavelengths (Eqs. (6) and (7)) and the numerical ones, for the sandwich configuration given in Table 1. One can notice the good agreement between theoretical and F.E. predictions for the two wrinkling loads and the similar behaviour of L_S and L_A for small thickness ratios. Moreover, in Léotoing et al. (2001b), it was shown that the wavelength of the local phenomena is independent of the boundary conditions and that the minimum of the two theoretical wavelengths leads to a correct magnitude of the element size in the simplified mesh.

The results of the F.E. and analytical models are coherent. The presented F.E. model permits to find out the three main buckling modes, thanks to a special attention in the modelling of the boundary conditions and loadings. The aim of the following part is to study the post-buckling regime for several configurations.

3. Numerical nonlinear analyses of the post-buckling regime

In this section, first the complete response of elastic sandwich beams is studied. This approach permits to classify the type of response as super- or sub-critical depending on the sandwich configuration. The so-called interactive buckling also receives a special attention since it affects the whole beam stability. Then different geometrical imperfections are introduced on a given configuration and their effects on the beam stability is studied. In the second part, an elastoplastic constitutive law is introduced for the core. This

approach is required when observing geometrical localizations in elastic cores which may turn out to be emphasized when nonlinear materials are considered.

3.1. Linear elastic materials

3.1.1. Sandwich configurations

The existence of a bifurcation point is related to a non-uniqueness of the solution which numerically cannot be simply dealt with. In order to solve numerically the post-buckling problem, it is necessary to turn it in such a way that a continuous response exists. This is possible, thanks to the introduction of a very small geometrical imperfection. For the following investigations, the geometrical imperfections are the linear buckling modes derived from the eigenvalue buckling predictions. Since eigenvectors are defined with an arbitrary magnitude, the maximum displacement component is chosen as the mode amplitude. As a result, the smaller the imperfection, the more 'exact' the post-buckling regime. The geometrical nonlinear analyses are led with ABAQUS™ and the use of a Riks algorithm permits to investigate the post-buckling problems both with stable and unstable behaviours. Indeed, this method considers the applied load as an additional unknown, the problem is then solved simultaneously for loads and displacements.

The construction of the design diagrams has permitted to isolate the configurations in which global buckling is predominant with respect to the local phenomena (configuration 3 in Fig. 12) and conversely (configuration 1 in Fig. 12). But a third zone can be defined in which the three buckling loads are very close. This optimum configuration, denoted configuration 2 in Fig. 12, is also prone to exhibit some interactions between the instabilities at the two scales of the material, as verified for instance by Byskov and Hutchinson (1977). Then, thanks to the design diagram presented in Fig. 12, built for the configuration $t_c = 50$ mm, $E_s = 70,000$ MPa, $E_c = 175$ MPa and $L = 470$ mm, the variation of the thickness ratio allows the selection of three configurations with very different buckling behaviours. The aim of the following paragraph is to identify the bifurcated branches for the three presented configurations by introducing a very small geometrical imperfection corresponding to the first eigenmode.

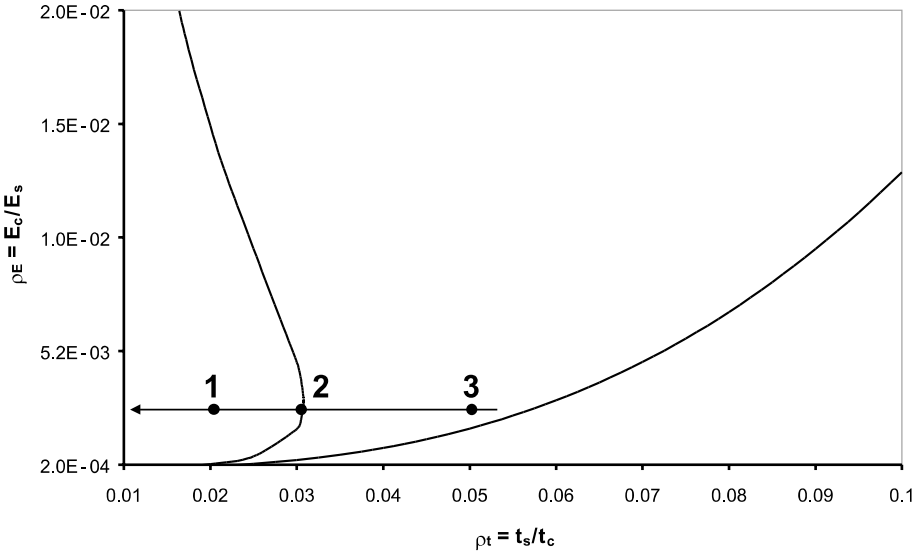

Fig. 12. Three geometrical and material sandwich configurations with different buckling behaviours.

3.1.2. Identification of the bifurcation branches

The numerical critical loads for the three configurations of Fig. 12 (t_s only varies) are given in Table 3. For the next plots, the change in the applied load (λ) is represented as a function of the global end shortening defined as the longitudinal displacement of the node where the load is applied in Fig. 6 normalized by the beam length ($u_1(L,t/2)/L$), or the global deflection defined as the transverse displacement of the node at mid-length and mid-thickness of the core normalized by the core thickness ($u_3(L/2,t/2)/t_c$). For the three configurations, the amplitude of the imperfection is 0.001 mm (0.0019% of the whole beam thickness).

Configuration 1 of Fig. 12 ($t_s = 1$ mm) is first considered. The lowest eigenvalue is associated with the antisymmetrical wrinkling mode for both analytical and numerical predictions (Table 3). A geometrical imperfection is then introduced on this local mode. Fig. 13 shows the corresponding load-end shortening response which exhibits two distinct regimes. The first part consists in a linear increase of the applied load versus the end shortening, up to the bifurcation point corresponding to the linear wrinkling load. After the bifurcation point, the post-buckling regime corresponds to an amplification of the antisymmetrical mode and the branch is super-critical (plate-like), i.e. the post-buckling regime of the sandwich beam is stable.

For configuration 2 in Fig. 12 ($t_s = 1.5$ mm), an imperfection associated with the critical global mode is introduced. The change in the applied load versus the global deflection is given in Fig. 14 which shows that the complete response can be divided into three parts. The first part corresponds to the fundamental 'flat' state of the beam undergoing only compressive deformations. The second part is associated with the post-

Table 3
Numerical linear buckling loads for the sandwich configurations presented in Fig. 12

	λ_{AG} (kN)	λ_{AL} (kN)	λ_{SL} (kN)
Configuration 1 ($t_s = 1$ mm)	115.1	96.8	96.9
Configuration 2 ($t_s = 1.5$ mm)	138.0	145.4	147.5
Configuration 3 ($t_s = 2.5$ mm)	167.5	219.7	262.4

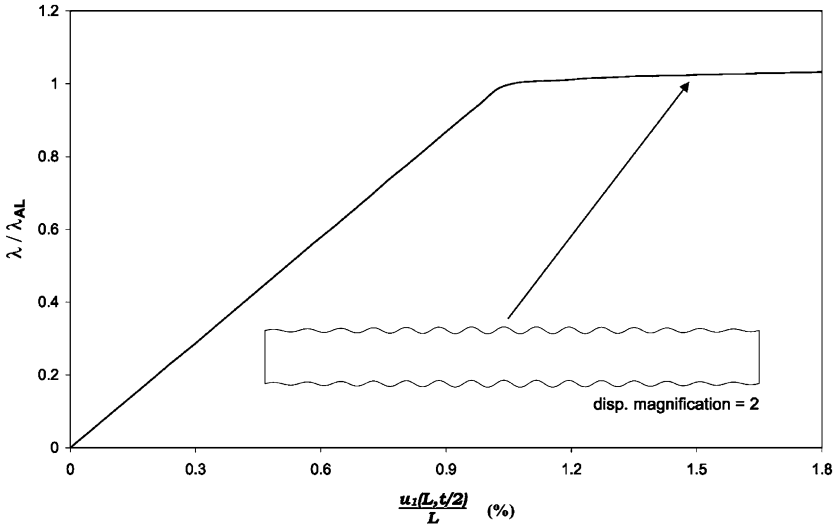

Fig. 13. Change in the applied load versus the global end shortening of the sandwich beam (configuration 1 of Fig. 12) for a geometrical imperfection of 10^{-3} mm on the antisymmetrical wrinkling mode.

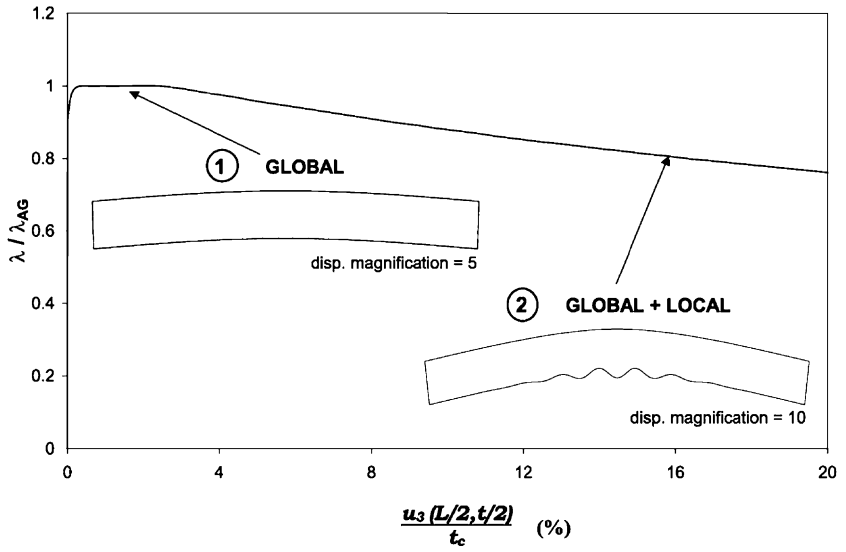

Fig. 14. Change in the applied load versus the global deflection of the sandwich beam (configuration 2 of Fig. 12) for a geometrical imperfection of 10^{-3} mm on the global mode.

buckling path of the equivalent homogeneous beam. This bifurcated branch is super-critical and the total applied load remains constant. The change in the deformed shape corresponds to the amplification of the global mode. But as the global deflection increases, and as it may be expected for this optimum configuration (Byskov and Hutchinson, 1977), a second bifurcation point is reached and the behaviour turns out to be strongly sub-critical (shell-like). The deformed shape of the sandwich beam is then made up of the previous global curvature onto which is superimposed a local wrinkling of the skin undergoing a compressive loading. The phenomenon of interactive buckling is here plainly illustrated. The interaction between the global mode and the wrinkling of one skin causes a geometrical localization responsible for a significant stiffness loss in the whole sandwich beam.

Finally, for the third configuration ($t_s = 2.5$ mm) a global imperfection is introduced, the corresponding load–deflection path is given in Fig. 15. Unlike the previous configuration, the amplitude of the global mode is amplified and no geometrical localization appears on the skins. This stable post-buckling behaviour is similar to that of the equivalent homogeneous sandwich beam.

3.1.3. Localization and stability

These first post-buckling investigations raise some interesting discussion points. To begin with, buckling modes and post-buckling regimes of a sandwich beam undergoing compressive loading are strongly dependent on its configuration. For configurations 1 and 3, in which, respectively, local and global buckling is predominant, the post-buckling behaviour is stable and only one bifurcation point is found. It must be noticed that the same geometrical imperfection can lead to two very different responses (global imperfection for configurations 2 and 3). This may, however, be due to the specificity of configuration 2, for which global and local critical loads are very close. In that case a form of interactive buckling is clearly observed and its harmful effects on the whole stability of the sandwich beam are demonstrated. Further investigations of this high imperfection-sensitive configuration are presented subsequently.

From this first approach, one can suggest that stability will depend on two main factors. The first one concerns the difference between the skin behaviours, i.e. when one skin is globally deformed while in the other one local phenomena develop. In this case, the sandwich beam is ‘unbalanced’, i.e. there is a breaking

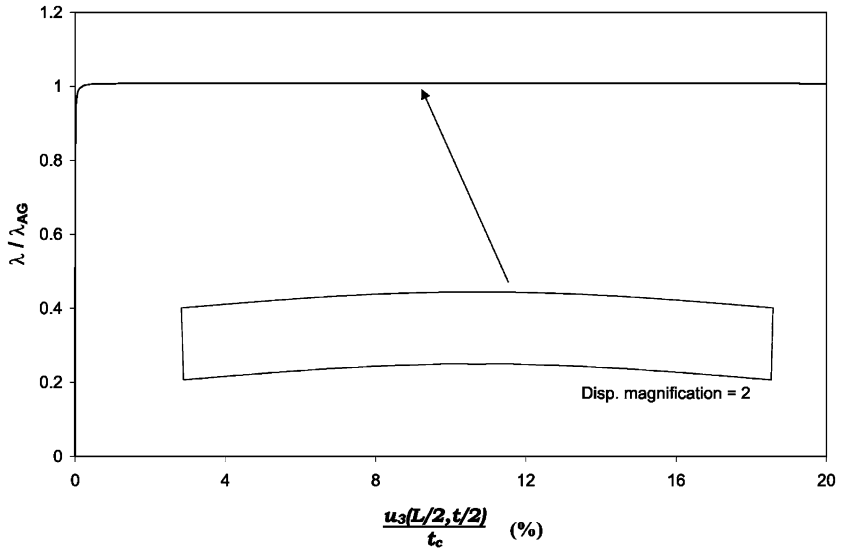

Fig. 15. Change in the applied load versus the global deflection of the sandwich beam for a global geometrical imperfection of 10^{-3} mm on sandwich configuration 3 of Fig. 12.

of the symmetry (Hunt et al., 1988), and unstable regimes are likely to develop. Second, the amplitude modulation (localization) along the deformed shape seems to play an important role, as it will be confirmed in the following part. About this localization of elastic deformations, a sensible analogy can be made with the post-buckling response of long one-dimensional beams resting on an elastic foundation (Wadee and Bassom, 2000). Indeed, the authors have shown that the periodicity of the deflected profile is characterized by a stable post-buckling behaviour. However, if periodicity is limited to a small region of the structure (sinusoidal bound by an exponentially decaying envelope, for example), the response will be sub-critical. One can expect this trend to be still emphasized when plasticity is considered (Tvergaard and Needleman, 1980).

3.1.4. Imperfection sensitivity

For the study of the imperfection sensitivity, various possibilities exist in the introduction of geometrical imperfections (form, size, combinations, etc.). The aim of this part is not to cover all the different cases, but simply to illustrate the main effects which can follow the introduction of a geometrical imperfection. Since interactive buckling may reveal most of the problems encountered separately in other configurations, sandwich configuration 2 in Fig. 12 is chosen and the three geometrical imperfections based on the three elastic buckling modes are, respectively, introduced. For the three cases, the amplitude of the imperfections are varied from 0.001 to 1 mm, that is to say from 0.0019% to 1.9% of the sandwich thickness. However, it is important to notice that the effects of a global geometrical imperfection with a given amplitude value are not directly comparable with the same local one. Indeed, for the global mode, an amplitude of 1 mm corresponds to a skin section rotation of 0.4° while for the symmetrical wrinkling, it becomes 8.4°. In this last case, the rotation magnitude is proportional to the wavenumber.

In Fig. 16, one can observe the variation of the applied load versus the global deflection of the sandwich beam for different values of the global imperfection amplitude. The first noteworthy point is that the existence of the two bifurcation points is still valid whatever the value of the geometrical amplitude. For the different imperfection values, the second branch remains unchanged and then a limit point in load is always

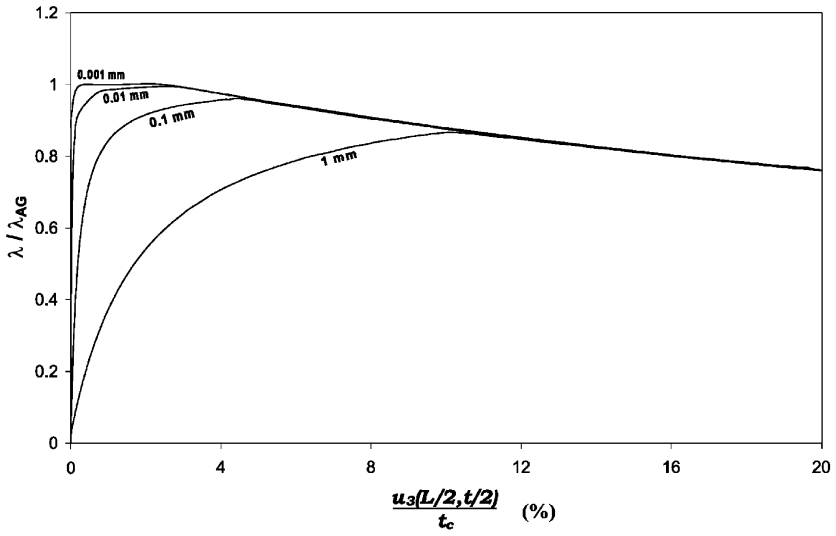

Fig. 16. Change in the applied load versus the global deflection of the sandwich beam for different global geometrical imperfection amplitudes in sandwich configuration 2.

reached. Therefore, by evaluating the first part of the post-buckling regime which corresponds to the behaviour of the equivalent homogeneous beam with a global imperfection, it is possible to find graphically the intersection between the two branches and to isolate the value of the maximum limit load. When increasing the imperfection, the value of the limit load decreases whereas the second bifurcation point deflection becomes larger. In Table 4, it can be seen that the drop in the limit load can be significant since for a rather low imperfection amplitude of 1 mm (1.9% of the total thickness), it exceeds 13%. Whereas the deflection associated with the second bifurcation point is multiplied by more than four for the same imperfection.

For the symmetrical imperfection (Fig. 17), the deformed shape is independent of the amplitude and still corresponds to an amplification of the symmetrical mode. Accordingly to the previous conclusions, as long as symmetry of the skins' behaviour is maintained and amplitude modulation is not significant, the global stability is ensured (by analogy with the antisymmetrical imperfection in configuration 1—Fig. 13). However, the effects of the symmetrical imperfection amplitude are particularly perceptible for low end shortenings (Fig. 17). For instance, increasing the imperfection amplitude from 0.001 to 1 mm induces a reduction by 2 of the load that can be withstood for an end shortening of 5 mm (1% of the beam length).

For the antisymmetrical imperfection case, the imperfection size effects are really noteworthy. Indeed, in addition to a drop in the limit load, the increase of the geometrical imperfection amplitude leads to some

Table 4
Change in the limit load and corresponding deflection for different values of the global imperfection amplitude in sandwich configuration 2

Global imperfection amplitude (mm)	*0.001*	*0.01*	*0.05*	*0.1*	*1*
Amplitude/total thickness (%)	*0.0019*	*0.019*	*0.096*	*0.19*	*1.9*
Limit load (kN)	140.2	139.2	136.6	134.6	121.4
Second bifurcation point deflection (mm)	1.25	1.58	2.00	2.48	5.39
Load decrease (%)	0	−0.7	−2.6	−4	−13
Deflection increase (%)	0	26	60	98	330

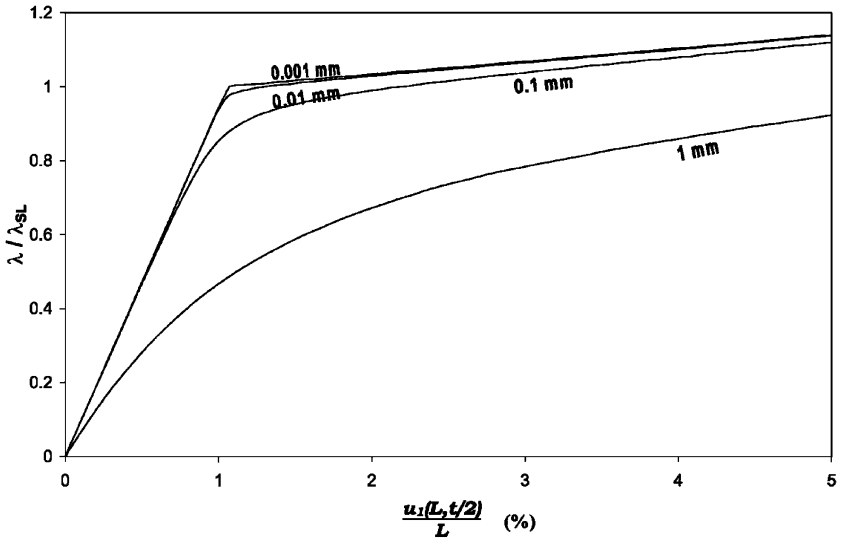

Fig. 17. Change in the applied load versus the global deflection of the sandwich beam for different amplitudes of the local symmetrical geometrical imperfection in sandwich configuration 2.

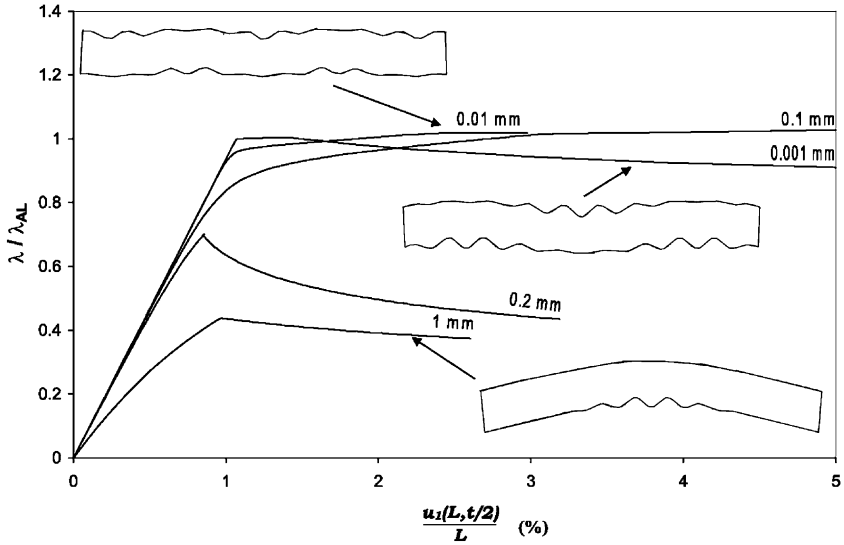

Fig. 18. Change in the applied load versus the global deflection of the sandwich beam for different local antisymmetrical geometrical imperfection amplitudes in sandwich configuration 2.

changes in the post-buckling response and then in the whole stability (Fig. 18). For a low amplitude of 0.001 mm, after a short plateau corresponding to stability, the post-buckling behaviour is slightly sub-critical and one can notice the existence of geometrical localizations on the two skins. Similarly to the same configuration but with global imperfection (Fig. 16), geometrical localization is associated with a drop in sandwich beam stiffness. But the presence of localizations on the two skins reduces here this drop, and the beam seems to be more 'balanced', i.e. the tendency of the beam is to remain straight and not to bend under

unbalanced localizations. This sub-critical behaviour is replaced by a super-critical regime for the imperfections of 0.01 and 0.1 mm in which the amplitudes are more comparable and the geometrical localization is less severe. For larger imperfection amplitudes (0.2 and 1 mm) again the interactive buckling revealed in Fig. 14 occurs, resulting in the superimposition of a global curvature and a local wrinkling of the skin under compression. In this last case, a limit point in load is reached and corresponds to only half of the eigen-buckling load.

In Fig. 18, one can observe the deformed shape for (an imperfection) amplitude of 0.01 mm. It is a form very close to the one with a 0.001 mm amplitude, but the beam seems to be more balanced and the stable post-buckling behaviour can be related to a lack of real localization, since the amplitude is almost constant. As a conclusion, when geometrical localizations develop, a sub-critical response of the sandwich beam is observed. Conversely, as long as the wave amplitude is not modulated, stability is maintained. The effect of geometrical localization is especially emphasized in cases where they do not appear in both skins, the more the localizations produce an unbalanced deformed shape, the sharper the sub-critical response.

Thanks to the different forms and sizes of the introduced geometrical imperfections, a sharp imperfection-sensitivity was noticed. This is first observed through the significant decrease of the maximum loads for sub-critical behaviours, but also by the possible change from a slightly super-critical regime to a severe sub-critical one for a very small increase in the antisymmetrical wrinkling size imperfection. These first analyses led with linear elastic materials have clearly emphasized the existence of stable and unstable post-buckling regimes. Unstable behaviours are related to the appearance of geometrical localizations along the beam. Since plastic deformation localization is known to be also responsible for sub-critical behaviours, especially in softening materials (Tvergaard and Needleman, 1980), it is essential to incorporate a nonlinear constitutive law in cores for which the hardening may be large.

3.2. Elastoplastic core and linear elastic skins

3.2.1. Constitutive model for the core

A rigid closed-celled PVC foam is considered here, chosen for the availability of its properties in the literature (Branner, 1995). The difficulty in modelling the foam constitutive laws lies in the existence of different deformation mechanisms in compression and in tension. In uniaxial compression, a stress–strain curve can be divided into three parts, a linear response is first observed, followed by a long plateau corresponding to the cell wall buckling and a last part associated with the densification of the foam in which cell walls interact and increase the global foam stiffness. Meanwhile the tensile stress–strain curves show a brittle behaviour for which the yield stress is greater than the compressive one.

A crushable foam model is implemented in ABAQUS™ (Aba, 1997; Martikainen and Rammerstorfer, 1999) which could meet our modelling needs. The yield surface can be built with different properties in tension and compression and the foam can deform volumetrically in compression which justifies the dependence of the yield function towards the hydrostatic stress in addition to the deviatoric ones. However, this model is rather delicate to calibrate and numerous convergence problems exist in the case of the foams which are of interest to us and which exhibit a tensile strength higher than the compressive strength. Consequently, in a first approach, a perfect elastoplasticity model is used with a von Mises yield function. The constitutive law is calibrated from uniaxial test in compression which is the most restricting behaviour for the foam. The densification part is not taken into account since it appears for very large strains (>40%) which were verified subsequently not to be reached in our computations.

3.2.2. Effects of the elastoplastic core behaviour on the post-buckling regimes

We can first consider sandwich configuration 2, studied in the previous section, in order to well underline the effects of the introduction of the core elastoplastic law. The chosen foam for the core is a Divinycell® H130 with a compressive and tensile modulus of 175 MPa and a compressive yield stress $\sigma_0 = 2.6$ MPa

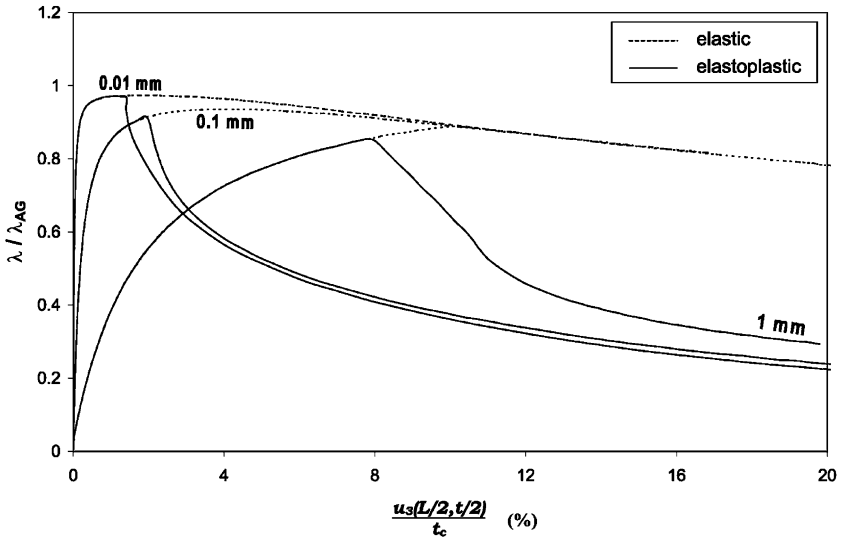

Fig. 19. Comparison of the change in the applied load versus the global deflection of the sandwich beam with a global imperfection, for elastic and elastoplastic constitutive law of the core.

(DIAB, 2001). The three previous geometrical imperfections are introduced and the effects of the core elastoplasticity are respectively discussed below. It must be noticed that due to the simplified F.E. formulation used, the complete elastoplastic post-buckling response of the 2000 d.o.f. sandwich beams is computed in about 20 min on the workstations described previously.

For a global geometrical imperfection, the evolution of the applied load versus the global deflection for different amplitudes is given in Fig. 19. The first noteworthy point is that the occurrence of a plastic flow is immediately followed by a drastic drop in the global stiffness of the sandwich beam. However, the value of the limit load is not really affected by this drop as it can be verified in Table 5. Concerning the deformed shape, after the bifurcation point, a strong localization of plastic deformations develop in the center of the sandwich beam (Fig. 20). The geometrical localization observed with an elastic core (Fig. 14) is here emphasized by the localization of plastic deformations.

The effects of the core elastoplasticity on the post-buckling behaviour of the sandwich beam with local symmetrical and antisymmetrical geometrical imperfections are, respectively, visible in Figs. 21 and 22. For the two cases, whatever the imperfection amplitude, the introduction of an elastoplastic constitutive law leads to a collapse of the sandwich beam. Experimentally, for the three forms of geometrical imperfection, the occurrence of the bifurcation point will be associated with the in-plane compressive strength of the beam, since neither a load control nor a displacement control will permit to reach an equilibrium without damaging the structure.

Table 5
Buckling load decrease between elastic and elastoplastic core for different values of the global imperfection amplitude in sandwich configuration 2

Global imperfection amplitude (mm)	*0.01*	*0.1*	*1*
Amplitude/total thickness (%)	*0.019*	*0.19*	*1.9*
Elastic limit load (kN)	133.4	128.2	121.8
Elastoplastic limit load (kN)	133.0	125.0	117.0
Load decrease (%)	−0.3	−2.5	−3.9

Fig. 20. Deformed shape and von Mises stress distribution in the sandwich beam (configuration 2) with elastoplastic core and global imperfection of 0.01 mm (deflection = 8 mm).

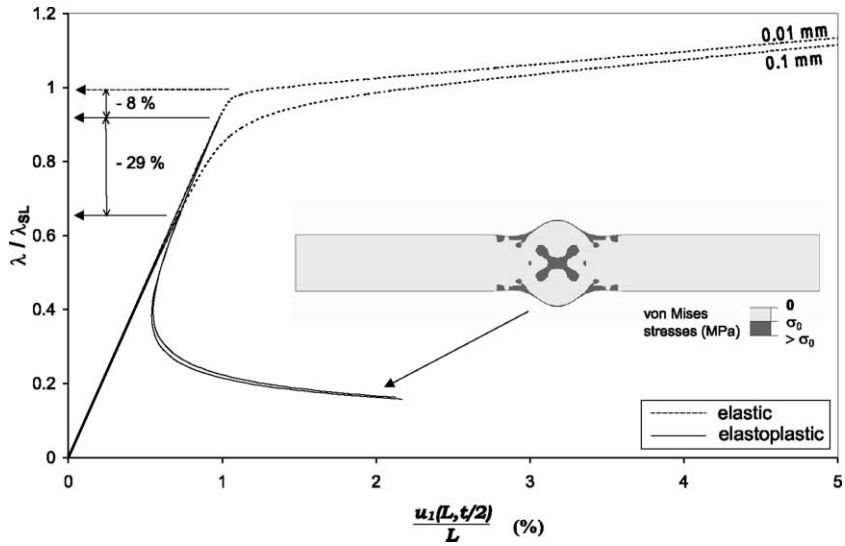

Fig. 21. Comparison of the change in the applied load versus the global deflection of the sandwich beam with sym-local imperfection, for elastic and elastoplastic core constitutive law.

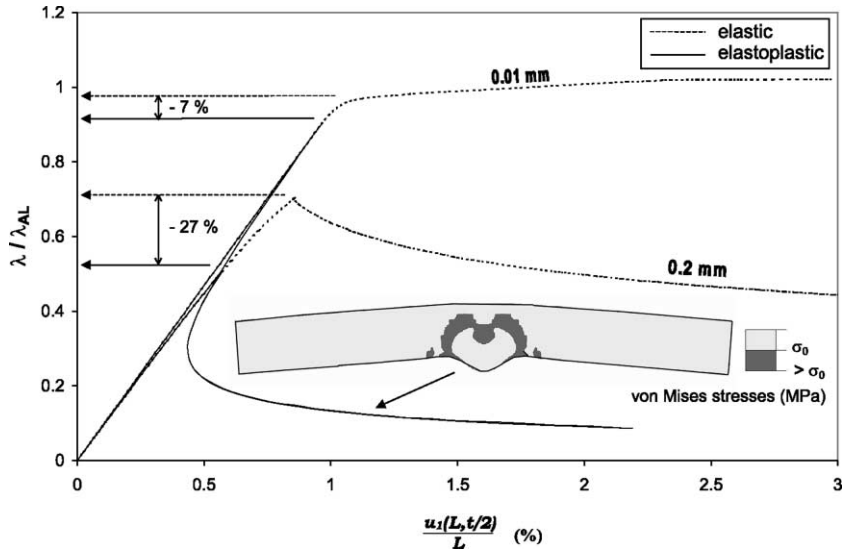

Fig. 22. Comparison of the change in the applied load versus the global deflection of the sandwich beam with anti-local imperfection, for elastic and elastoplastic core constitutive law.

For the two last cases (Figs. 21 and 22), the first important point is that the greater the imperfection amplitude, the larger the decrease of the observed critical load. Indeed, by increasing the imperfection amplitude from 0.01 to 0.1 mm, the limit load in comparison with the one for an elastic core has decreased from about 10% to 30% in both antisymmetrical and symmetrical cases. Furthermore, the post-bifurcated branch associated with the plastic flow is independent towards the imperfection size, and for the antisymmetrical case (Fig. 22), the elastic super and sub-critical behaviours observed in Fig. 18 are both replaced by the same bifurcated branch. For the deformed shape, a strain localization appears in the center of the beam. The initial symmetrical configuration maintains its symmetry while for the antisymmetrical form a global curvature appears due to the localization of deformations. A last point is that the distribution of the core von Mises stresses in Fig. 21 clearly demonstrates the predominance of shear in the plastic flow.

Eventually, for any imperfection, the response is highly sub-critical associated with strong plastic deformation localizations: responses which are stable with an elastic core are prone to undergo plastic deformation localization, while sub-critical responses caused by geometrical localization are further aggravated when the core plasticity is accounted for. One can assimilate this behaviour to shells' plastic buckling, the response of which is sub-critical and highly imperfection sensitive.

3.2.3. Shear crimping: a special case of global buckling

The previous numerical investigations have been made for sandwich configuration 2 of Fig. 12. In the present section, a global imperfection is introduced in a sandwich beam in which global buckling is prone to appear first (configuration 3 in Fig. 12). Calculations with a linear elastic constitutive law in the core have shown that whichever the size of the imperfection, the post-buckling regime is stable and corresponds to an amplification of the global buckling mode (Figs. 15 and 23). In this case, the post-buckling behaviour is that of the equivalent homogeneous beam without any local effect from the skins. The introduction of the elastoplastic law in the core affects this post-buckling behaviour and the occurrence of plastic flow gives rise to a strong drop in the global stiffness of the beam (Fig. 23). The corresponding deformed sandwich beam (Fig. 23) clearly exhibits a localization of the shear deformations in the beam, this is the so-called *shear crimping*. Shear failure will presumably appear in this region of weakness where the transverse shear stresses

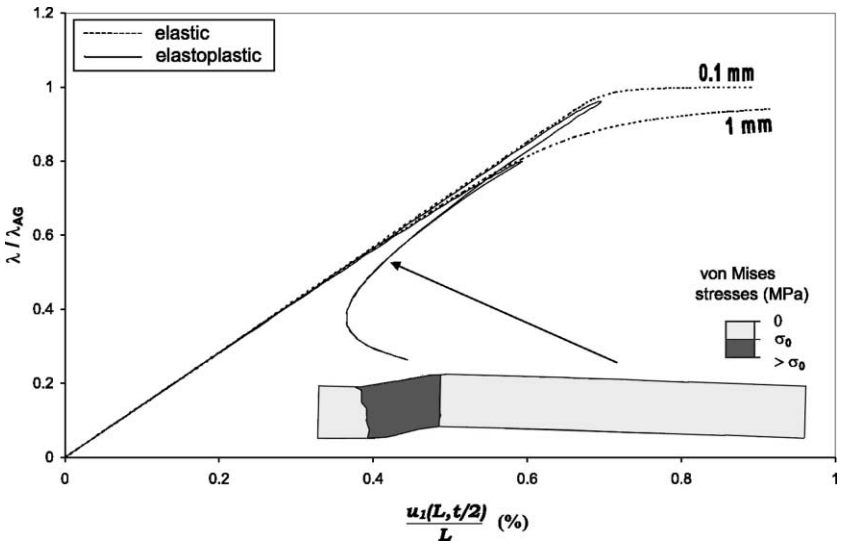

Fig. 23. Comparison of the change in the applied load versus the global deflection of the sandwich beam with global imperfection, for elastic and elastoplastic core constitutive law (sandwich configuration 3 of Fig. 12).

are maximum. This region is localized between the quarter of the beam length and its extremity, which are the zones of maximum shear stress, respectively, for a beam with clamped ends and for a simply supported beam. This last observation is in agreement with the F.E. model used in which edges are slightly stiffened by the chosen boundary conditions. In literature (Allen, 1969), the shear crimping is associated with a critical load which in fact corresponds to the equivalent transverse shear stiffness of the sandwich beam:

$$\lambda_{\text{shear}} = \frac{G_c b (t_c + t_s)^2}{t_c}. \tag{8}$$

In Fig. 23, one can observe that a limit load is reached when the shear crimping appears. This load is very sensitive to the size of the initial imperfection since for an imperfection of 1 mm, the decrease is 17% in comparison with a 0.1 mm imperfection amplitude. The value of λ_{shear} for the chosen geometrical and material parameters is 2.2×10^5 N. The limit loads computed for the two tested imperfection amplitudes (0.1 and 1 mm) correspond, respectively, to 70% and 60% of this too large value of the shear crimping load.

Eventually, due to the high numerical sensitivity of shear crimping towards the imperfection size and because of the large overestimation of λ_{shear}, Eq. (8) cannot be used as a design criterion against this phenomenon. Indeed, shear crimping is strongly dependent on the elastoplastic nature of the core material and cannot be accurately predicted by a simple combination of geometrical and material parameters. All the numerical investigations carried out have shown that shear crimping is in fact a consequence of the shear deformation localization following the occurrence of a global mode. This may explain why this phenomenon is very often considered as a special case of global buckling. Besides, the large influence of the imperfection amplitude on the value of the limit load justifies the problems met in the experimental characterization of shear crimping.

4. Conclusion

This study has been divided into two parts. The first part was dedicated to the characterization of sandwich beam instabilities in a perfect linear framework. It was shown that this simplified framework permits to identify, from a specific unified model, analytical criteria associated with both local and global instabilities. Thanks to these expressions, very rich conclusions can be drawn regarding the buckling modes at the two scales of a sandwich. Design diagrams were built and clearly demonstrated that local phenomena are predominant in sandwich beam made up of weak and thick cores, whereas global buckling prevails in slender beams. In order to lead more complex and realistic numerical analyses, a low CPU time-consuming simplified model was assessed. The numerical eigenvalue buckling predictions were shown to correlate very well the analytical results.

The second essential step was to characterize the post-buckling response of sandwich beams in order to identify the main bifurcation branches and then to isolate the configurations developing super- or sub-critical post-buckling behaviours. The geometrical nonlinear investigations, in which linear elastic materials are considered, have actually revealed the existence of stable and unstable post-buckling regimes. Unstable behaviours are related to the occurrence of geometrical localizations along the beam. This is still emphasized when localizations do not develop symmetrically on both skins, inducing a breaking of the symmetry that leads to a drastic drop of the load carrying capacities. A special case of 'unbalanced' buckling is the so-called interactive buckling, occurring in optimum configurations for which the critical loads are close. Interactive buckling yields a post-buckling behaviour highly sub-critical whereas it results from the interaction of global and local modes inherently stable. Besides, a very high sensitivity towards the imperfection sizes and forms was observed. The introduction of an elastoplastic constitutive law in the core emphasizes the sub-critical response observed in many cases with elastic materials. Plastic flows appear at

the onset of the instability occurrence, leading to very sub-critical regimes, followed by the development of plastic strain localization. Moreover, for some configurations, the value of the limit load from the elastoplastic analysis is strongly lower, up to 30%, than for linear elastic materials. The consideration of core elastoplasticity is then critical for these cases, as well as in the cases prone to exhibit interactive buckling.

Through these analyses, a very high sensitivity towards imperfections was demonstrated which corroborates the strong difficulties in obtaining reproducible experimental results. This is especially true for the characterization of shear crimping which was shown to be a post-bifurcated phenomenon that will appear in configurations in which global buckling is predominant.

Following the conclusions of Tvergaard and Needleman (1980) for inherently super-critical structures made up of elastoplastic materials, local imperfections will not affect significantly the load carrying capacity of the sandwich beam. Hence studying the maximum support load in the case of periodic modes and imperfections is still valid. Consequently, the complete analytical characterization of the elastic interactive buckling in sandwich is under achievement with the presented unified model.

References

Aba, 1997. ABAQUS Theory Manual. Hibbitt, Karlsson & Sorensen.

Allen, H., 1969. Analysis and Design of Structural Sandwich Panels. Robert Maxwell, MC, MP.

Branner, K., 1995. Capacity and lifetime of foam core sandwich structures. PhD thesis, Technical University of Denmark.

Byskov, E., Hutchinson, J., 1977. Mode interaction in axially stiffened cylindrical shells. AIAA Journal 15 (7), 941–948.

DIAB, 2001. Divinycell H grade. Technical Report, DIAB group.

HEXCEL, 1989. Mechanical properties of hexcel honeycomb materials. Technical Report TSB120.

Hunt, G., Da Silva, L., Manzocchi, M., 1988. Interactive buckling in sandwich structures. Proceedings of the Royal Society of London A 417, 155–177.

Leger, A., Combescure, A., Potier-Ferry, M., 1998. Bifurcation, flambage, stabilité en mécanique des structures. Technical Report, IPSI.

Léotoing, L., Drapier, S., Vautrin, A., 2001a. A novel unified model for sandwich: closed-form solutions for global and local buckling of beams. European Journal of Mechanics A/SOLIDS (submitted).

Léotoing, L., Drapier, S., Vautrin, A., 2001b. Using new closed-form solutions to set up design rules and numerical investigations for global and local buckling of sandwich beams (submitted).

Lo, K., Christensen, R., Wu, E., 1977. A high-order theory of plate deformation, part 1: homogeneous plates. Journal of Applied Mechanics, 663–668.

Martikainen, L., Rammerstorfer, F., 1999. Modelling the local failure modes in thin-faced sandwich panels. Strojnícky Časopsis 50, 241–252.

Sokolinsky, V., Frostig, Y., 1999. Boundary condition effects in buckling of "soft" core sandwich panels. Journal of Engineering Mechanics 125 (8), 865–874.

Starlinger, A., 1990. Development of efficient finite shell elements for the analysis of sandwich structures under large deformations and global as well as local instabilities. PhD thesis, Vienna University of Technology.

Teti, R., Caprino, G., 1989. Mechanical behavior of structural sandwiches. In: Olsson, K., Reichard, R. (Eds.), Proceedings of Sandwich Constructions 1. Engineering Materials Advisory Services Ltd., pp. 53–68.

Tvergaard, V., Needleman, A., 1980. On the localization of buckling patterns. Journal of Applied Mechanics 47, 613–619.

Vinson, J., 1989. Comparison of optimized sandwich panels of various constructions subjected to in-plane loads. In: Olsson, K., Reichard, R. (Eds.), Proceedings of Sandwich Constructions 1. Engineering Materials Advisory Services Ltd., pp. 23–52.

Wadee, K.M., Bassom, A.P., 2000. Restabilization in structures susceptible to localized buckling: an approximate method for the extended post-buckling regime. Journal of Engineering Mathematics 38 (1), 77–90.

Williams, D., Leggett, D., Hopkins, H., 1941. Flat sandwich panels under compressive end loads. Technical Report, 1987, R.A.E.